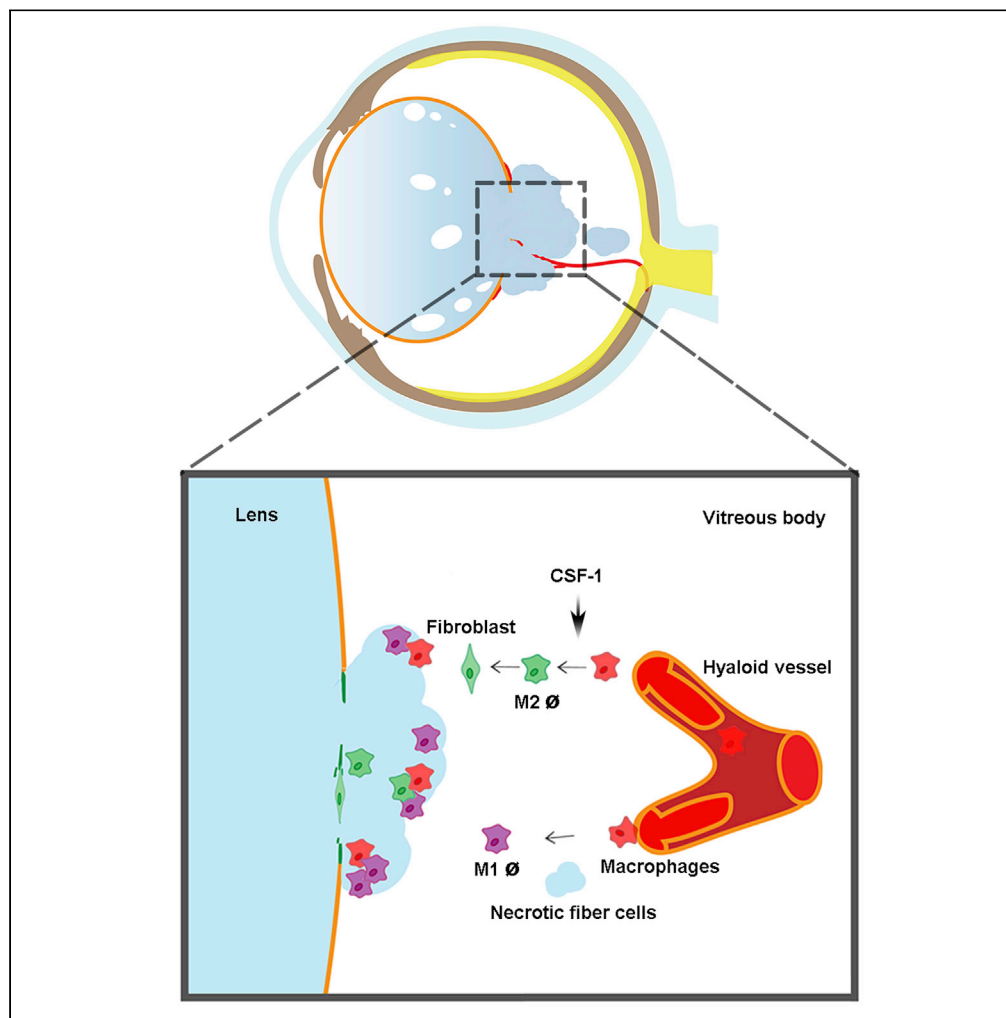**Article**

# Macrophage recruitment in immune-privileged lens during capsule repair, necrotic fiber removal, and fibrosis



Yuting Li, Zhen Li, Yumeng Quan, ..., Xiao-Dong Li, Sumin Gu, Jean X. Jiang

jiangj@uthscsa.edu

### Highlights
Lens posterior rupture delays regression of the hyaloid vessels.

Lens posterior rupture recruits macrophages delivered by the hyaloid vessels.

Macrophages mediate necrotic fiber cell removal and capsule rupture sealing.

CSF-1 activated M2 macrophages facilitate capsular rupture sealing by fibrosis.

**Article**

# Macrophage recruitment in immune-privileged lens during capsule repair, necrotic fiber removal, and fibrosis

Yuting Li,[1,2,4] Zhen Li,[2] Yumeng Quan,[2] Hongyun Cheng,[2] Manuel A. Riquelme,[2] Xiao-Dong Li,[3] Sumin Gu,[2] and Jean X. Jiang[2,5,*]

## SUMMARY

**Emerging evidence challenges the lens as an immune-privileged organ. Here, we provide a direct mechanism supporting a role of macrophages in lens capsule rupture repair. Posterior lens capsule rupture in a connexin 50 and aquaporin 0 double-knockout mouse model resulted in lens tissue extrusion into the vitreous cavity with formation of a "tail-like" tissue containing delayed regressed hyaloid vessels, fibrotic tissue and macrophages at postnatal (P) 15 days. The macrophages declined after P 30 days with M2 macrophages detected inside the lens. By P 90 days, the "tail-like" tissue completely disappeared and the posterior capsule rupture was sealed with thick fibrotic tissue. Colony-stimulating factor 1 (CSF-1) accelerated capsule repair, whereas inhibition of the CSF-1 receptor delayed the repair. Together, these results suggest that lens posterior rupture leads to the recruitment of macrophages delivered by the regression delayed hyaloid vessels. CSF-1-activated M2 macrophages mediate capsule rupture repair and development of fibrosis.**

## INTRODUCTION

The lens has long been defined as an immune-privileged organ in which direct lymphatic drainage is missing and immune cell entry is strictly prohibited (Medawar, 1948; Godwin and Brockes, 2006; Taylor and Kaplan, 2010). The lens, as an avascular ocular tissue, depends on nutrients provided by the aqueous humor in the anterior chamber and vitreous humor in the posterior chamber of the eye. In the anterior chamber, the aqueous humor contains various neuropeptides and molecules, as well as cell surface protein Fas ligand, to suppress the activation of immune cells (Taylor and Kaplan, 2010). The vitreous cavity, similar to the anterior chamber, possess the vitreous cavity-associated immune deviation (Sonoda et al., 2005; Streilein, 2003). Previous studies have suggested that the lens is also subject to immune cells surveillance and invasion. Immune cells could be recruited to two immune privileged tissues, the cornea and lens, after injury (Logan et al., 2017; Pal-Ghosh et al., 2014; Shechter et al., 2013). After injury, innate immune cells in the peripheral cornea are reported to be quickly activated and migrate to the central cornea (Lee et al., 2010; Pal-Ghosh et al., 2014; Sica and Mantovani, 2012). A recent study found that lens degeneration provoked an immune response, which is also elicited in other ocular tissues including the cornea, vitreous, and retina (Logan et al., 2017). It is further speculated that the immune cells in the lens are likely released from the ciliary body and that the immune response may contribute to fibrosis in response to injury.

The lens comprises two cell types: a single layer of epithelial cells under the anterior capsule and differentiated fiber cells making up the bulk of the lens organ. Lens growth is driven by the continuous proliferation and differentiation of epithelial cells in the equatorial region that form nascent fiber cells. Three connexins have been identified in the vertebrate lens: Cx43 and Cx50 in epithelia cells, and Cx46 and Cx50 in the bulk of fiber cells (Kistler et al., 1985; Paul et al., 1991; White et al., 1992). These connexins that form gap junctions connecting the cytoplasm of neighbor cells and allowing passage of small molecules are important for lens homeostasis and transparency. Aquaporin 0 (AQP0) is the most abundant membrane protein expressed in lens fibers and plays an essential role in lens transparency (Varadaraj et al., 1999; Kumari et al., 2011). We have previously shown that Cx50 directly interacts with AQP0 in lens fibers in the embryonic and young lens, and this interaction promotes gap junction channel activity (Hu et al., 2017; Liu et al., 2011; Yu and Jiang, 2004; Yu et al., 2005). Many gene mutations of Cx50 and AQP0 have been identified and are

[1]Department of Ophthalmology, Lanzhou University Second Hospital, Lanzhou, Gansu 730000, China

[2]Department of Biochemistry and Structural Biology and, University of Texas Health Science Center, San Antonio, TX 78229-3900, USA

[3]Department of Microbiology, Immunology and Molecular Genetics, University of Texas Health Science Center, San Antonio, TX 78229-3900, USA

[4]Second Clinical School, Lanzhou University, Lanzhou, Gansu 730000, China

[5]Lead contact

*Correspondence: jiangj@uthscsa.edu

https://doi.org/10.1016/j.isci.2021.102533

directly associated with congenital cataracts in humans (Jiang, 2010; Chepelinsky, 2009). Similar cataract phenotypes are also observed in Cx46, Cx50, AQP0 knockout (KO) or mutated gene knock-in mouse models (White et al., 1998; Al-Ghoul et al., 2003; Lo et al., 2014; Gong et al., 1997). By generating an AQP0/Cx50 double-KO (dKO) mouse model, we show that Cx50 and AQP0 play important roles in mediating cell-cell adhesion in lens fibers, and their deficiency impairs fiber organization, integrity, mechanical properties, and lens development (Gu et al., 2019). Moreover, lens fiber cells in dKO mice "leak" out of the lens through the ruptured posterior capsule.

Macrophages, a key cell type of the immune system, are classified as activated macrophages (M1) and alternatively activated macrophages (M2) (Duffield et al., 2005; Lang and Bishop, 1993; Martinez et al., 2008). M1 macrophages play a major role as proinflammatory and tissue-destroying cells (Gratchev et al., 2006; Martinez et al., 2008). In contrast, M2 macrophages induce anti-inflammatory/profibrotic cytokines, which reduce inflammatory responses, and promote tissue remodeling and fibrosis (Gratchev et al., 2006; Sica and Mantovani, 2012). In this study, we report a direct mechanism in which macrophages delivered by delayed regressed hyaloid vessels are activated and recruited by necrotic lens fiber cells in response to the ruptured posterior lens capsule in the Cx50/AQP0 dKO mouse model. The M2 macrophages, activated by colony-stimulating factor 1 (CSF-1), facilitate necrotic fiber cell removal, capsule rupture repair, and fibrosis. This study provides direct evidence supporting a key role played by macrophages in response to damaged lens cells in an immune-privileged organ.

## RESULTS

### Extrusion of lens fiber tissues through the ruptured posterior capsule in Cx50/AQP0 dKO mice

Our previous studies have shown a significant reduction in the eyeball and lens size in Cx50KO and Cx50/AQP0 dKO mice compared with wild-type (WT) and AQP0KO mice (Gu et al., 2019). Here, we found that the increase in lens mass and diameter of the dKO was delayed during postnatal (P) development, and the growth rate was significantly less than those of WT and single KO, especially compared with WT and AQP0 KO groups (Figures S1A and S1B). Interestingly, compared with WT, the weight-to-volume ratio of dKO lenses was reduced at P 30 days (Figure S1C). These results suggest that the loss of lens mass is possibly caused by fiber cells extruded out of the lens via the ruptured posterior capsule. Indeed, enlarged, empty extracellular spaces were observed, and the percentage of the empty spaces associated with lens development was increased (Figure S1D).

Compared with WT, AQP0, and Cx50 single KO, dKO lenses exhibited a wide range of lens posterior defects, including posterior polar cataracts, posterior capsule rupture, and posterior lens fiber tissue extrusion with the formation of a "tail-like" tissue mass with hyaloid vessels (Figures 1A and 1B). We compared corresponding lens areas in WT and dKO across various P developmental stages (Figure S2A). Most of the posterior capsules of dKO lenses were ruptured at P 15 days, and lens fiber tissues were subsequently "leaked" out of ruptured posterior capsules into the vitreous cavity (Figure S2A). The lens regions, as illustrated in Figure S2B, included epithelial cells (Figure S2C) and differentiating fiber cells at the equator (Figure S2D), central (Figure S2E) and posterior regions (Figure S2F) of WT and dKO mice from P 1 to 60 days. In contrast to the subtle changes at P 1 day, P 7-day dKO lenses showed distinct morphological changes, including increased empty spaces (black asterisk, Figure S2C) in the anterior and central nuclear regions, disrupted sutures, and delayed denucleation of lens fiber cells (black ar, P 7 days, Figure S2E). In addition to enlargement and disorganization of lens fiber cells, ~ 55% of posterior capsules were ruptured with fiber cells extruded out of the lenses (P 7 days, Figure S2F). At P 15 days, a significant delay in lens differentiation and impaired nuclei degradation (black ar) was observed in outer cortical fibers. In this region, enlarged, distorted fiber cells appeared to migrate toward the posterior lens capsule. At P 15 days, we detected increased extracellular spaces (asterisk) underneath the epithelial cells (Figure S2C), at the lens equator (Figure S2D), and central nuclear regions (Figure S2E). Ruptured posterior capsules with the "tail-like" tissue were seen in ~95% of dKO lenses. The fiber tissues were extruded out of the lens and expanded into the vitreous cavity (Figure S2F). By P 30 days, a further increase of intercellular spaces was seen in the anterior lens region (Figure S2C), which was associated with abnormal nuclear distribution, various enlarged intercellular spaces, and necrotic central lens regions (Figure S2E, black arrow). Distinctively, at P 30 days, the morphology of fiber cells appeared to be totally altered, resulting in an unrecognizable tissue mass (Figure S2E). In addition, posterior "tail-like" tissues were reduced and replaced by fibrotic tissue (Figure S2F). At P 60 days, epithelial cells lost cell polarity, and some areas were double layered with cytoplasmic
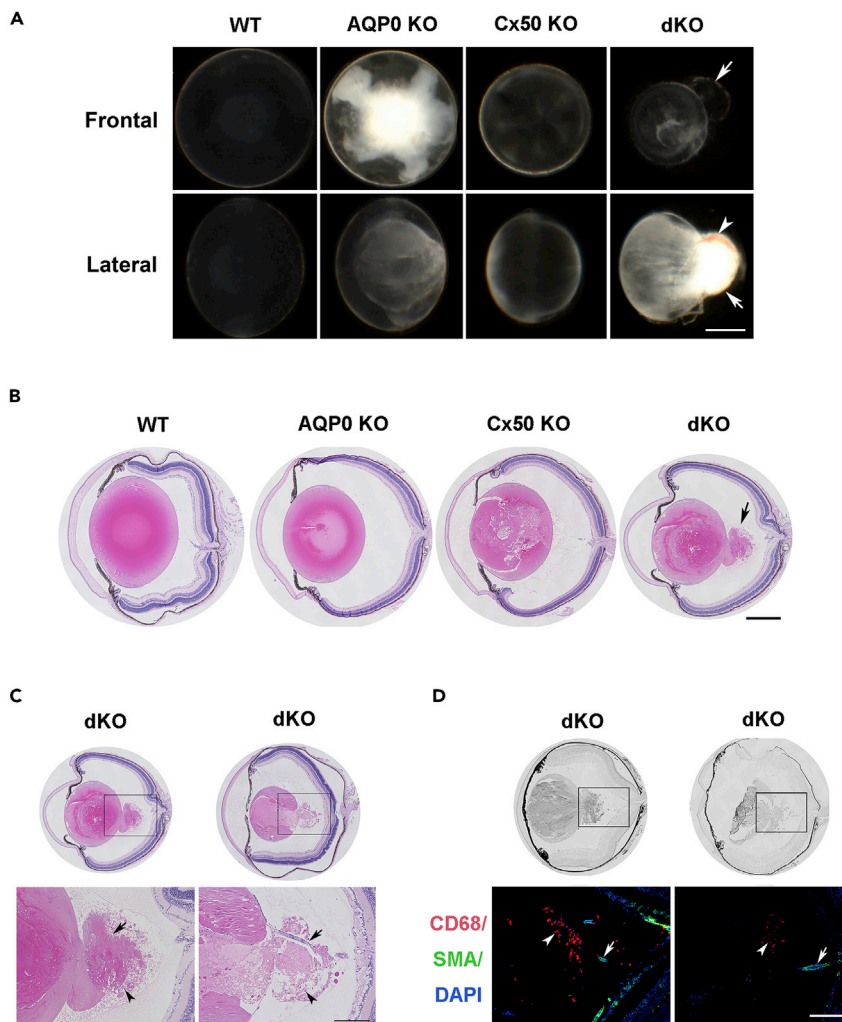
**Figure 1. Mice deficient in Cx50 and AQP0 develop a "tail-like" tissue mass at the lens posterior region**

(A) The frontal and lateral images of P 15 days lenses of WT, AQP0 KO, Cx50 KO, and Cx50/AQP0 double knockout (dKO) mice. Cataracts were found in all three types of knockout mice, but only dKO mice showed a "tail-like" tissue extrusion (white arrow) and blood vessels (white arrowhead) in the posterior part of lens. Scale bar = 500 μm.

(B) Hematoxylin and eosin (H&E) staining of paraffin sections of the eye showed the posterior capsule rupture (black arrow) only in dKO mice. Scale bar = 500 μm.

(C) H&E staining of paraffin sections of the eye showed that "tail-like" tissue extrusion consisted of distorted lens fiber cells, hyaloid vessels (black arrow), fibrotic tissue, and some infiltrated cells (black ar). Scale bar = 200 μm.

(D) Cryosections of eyes were coimmunofluorescence stained with CD68 antibody (red), α-smooth muscle actin antibody (α-SMA) (green), and DAPI (blue). Macrophages (white ar) surrounding the "tail-like" tissue and hyaloid vessels (white arrow) in the vitreous cavity. Scale bar = 200 μm.

vacuoles (Figure S2C). Moreover, the appearance of large infiltrated multinucleated macrophages (empty black arrow) was detected in the central lens region (Figure S2E). Approximately 56% of the posterior capsules were sealed by fibrotic tissue (Figure S2F).

About 55% of posterior capsule ruptures were detected by P 7 days and increased to 95% at P 15 days (Table 1). Lenses with "tail-like" tissues increased to 83% at P 30 days, decreased to 43.8% at P 60 days and further decreased to 17% at P 90 days (Table 2). The "tail-like" tissue in dKO lenses appeared to comprise lens fiber cells, vascular vessels, fibrotic tissues, and infiltrated cells (Figure 1C). A vessel (indicated by an arrow in the bottom right panel) appeared to trespass the "tail-like" tissue and connect the lens posterior to the optic nerve in dKO mice. To identify the infiltrated cells, we used CD68 antibody and α-smooth muscle actin (α-SMA) antibody to label macrophages and vessels, respectively (Figure 1D). CD68^{+} macrophages

**Table 1. Posterior capsule ruptured at P 1, 7, and 15 days**

|  | P 1 day (n = 9) | P 7 days (n = 11) | P 15 days (n = 21) |
|---|---|---|---|
| WT | 0 | 0 | 0 |
| dKO | 0 | 54.6% | 95.2% |

were detected around the "tail-like" tissue at P 15 days in the dKO lens. The presence of vessels was also confirmed by α-SMA expression. These results show that "tail-like" lens tissue extruded from ruptured posterior lens capsules in dKO mice is infiltrated with blood vessels and macrophages.

### Delayed regression of hyaloid vessels in dKO lens

Besides posterior capsular rupture, the regression of the hyaloid vessel system in the dKO lens was delayed. We observed that contrary to the hyaloid vessel regression in WT at P 15 days (Figure 2A). The hyaloid artery (HA) was still present in the dKO lens and associated with fibrotic tissue, even at P 60 days (arrow). A large amount of fibrotic tissue was also present in the posterior region of the dKO lens. We followed the histological changes of hyaloid vessels in WT and dKO mice up to 1 year. At P 60 days, the posterior capsule was repaired while fibrosis was increased (ar). After P 120 days, the hyaloid vessel system completely regressed and was replaced by fibrotic tissue (ar). These fibrotic tissues remained and were detected in 1-year-old dKO mice. To determine the relationship between the vessels and macrophages, we performed immunostaining with anti-SMA antibody and costained with CD68 antibody (Figure 2B). The hyaloid vessel system was detected at P 15 days in the vitreous cavity, which included the HA (white solid arrow), hyaloidea propria (white asterisk), and tunica vasculosa lentis (white ar, Figure 2B), and the vessels were still present at P 60 days. Some CD68$^+$ macrophages appeared to associate with the vessels. These data indicate that macrophages are likely delivered by delayed regressed hyaloid vessels.

To assess the role of macrophages around the "tail-like" tissue, we coimmunostained with antibodies against CD68 and the lens fiber cell membrane protein, Cx46 (Figure 2C). Various-shaped macrophages at various time points were detected, and interestingly, debris of lens fiber cells indicated by Cx46-postive signaling was found inside the macrophages (solid white ar, Figure 2C). At P 15 and 30 days, more pseudopodium structures (solid white arrow, Figure 2C) appeared extending from the cell surface of macrophages, which may assist cell migration (Mathias et al., 2009). At P 60 and 90 days, more macrophages changed to an ovoid shape or fused into multinucleated, giant cells (Figure 2C). Moreover, macrophages were firstly located around the "tail-like" tissue at P 15 days and then migrated inside the lens after P 30 and 60 days. Quantification analysis showed that the number of CD68$^+$ macrophages in the "tail-like" tissue of P 30-day and P 60-day groups was significantly decreased as compared with that in the P 15-day group (p = 0.015 and p = 0.003, respectively). In contrast, compared with those in the P 15-day lens, the numbers of CD68$^+$ macrophages inside the P 30-day and P 60-day lens were significantly increased (p = 0.02 and p = 0.002, respectively) (Figure 2D). The data indicate that macrophages are recruited and delivered by hyaloid vessels to the "tail-like" tissue that is associated with posterior capsular rupture and subsequently engulf lens fiber cells. Macrophages appear to mediate the clearance of the "tail-like" tissue mass outside the lens and continue to migrate into the lens. At this stage, we also observed the regression of the hyaloid vessel system.

### Recruitment of macrophages by necrotic fiber cells in the dKO lens

We sought to determine what drives macrophages to immune-privileged lens tissues. Macrophages can respond to cell death during tissue damage (Chazaud, 2014). Immunostaining with Cx46, caspase-3, and CD68 antibodies was used to examine the apoptotic lens tissues and their relationship with macrophages (Figure S3). At P 15 and 30 days, some of the Cx46-positive fiber cells inside the lens were labeled with caspase-3, and these cells were mostly localized around outer cortical lens fibers in the WT lens (Figure S3A). However, in the dKO lens, enhanced caspase-3-positive cells were detected across lens fiber cells, particularly at central, posterior fiber regions (Figure S3B), and at the "tail-like" tissue mass (Figure S3C). Moreover, the CD68$^+$ macrophages were located around caspase-3$^+$ lens fiber cells. Caspase-3$^+$ cells expanded at P 30 days and colabeled with lens fiber protein Cx46 (Figures S3A and S3B, lower panels; Figure S3C, top panel). However, in some regions, the colocalization was less evident (Figure S3C, middle panel), possibly caused by the cleavage of the Cx46 C-terminal antigen site by caspase-3 (Yin et al., 2001, 2008). Nevertheless, CD68$^+$ macrophages appear to primarily associate with apoptotic lens fiber cells.

**Table 2. "Tail-like" tissues existed at P 30, 60, and 90 days**

|  | P 30 days (n = 18) | P 60 days (n = 16) | P 90 days (n = 12) |
|---|---|---|---|
| WT | 0 | 0 | 0 |
| dKO | 83.3% | 43.8% | 16.7% |

In addition to its role in apoptosis, caspase-3 plays an important role in lens differentiation in the outer lens regions containing differentiating fibers (Zandy et al., 2005). To circumvent the potential issue associated with caspase-3 as a differentiation marker in the lens, we used another apoptotic marker, caspase-8. In addition, caspase-8$^+$ apoptotic cells are thought to be the precursor of receptor-interacting-protein-kinase-3 (RIP3)-positive necrotic cells. RIP3 is a protein kinase that functions in necrosis induced by physiological stimuli and induces or enhances necrosis (Moriwaki and Chan, 2013; Sun et al., 1999). Expression of RIP3 is crucial for switching apoptosis to necrosis (Zhang et al., 2009). Because necrotic cells are reported to be a trigger for recruiting macrophages (Chazaud, 2014), we examined WT and dKO mice lenses for levels of apoptosis and necrosis of lens fiber cells at various P developmental stages (Figure 3). Coimmunostaining with CD68 and caspase-8 antibodies showed that CD68$^+$ macrophages accumulated and located close to caspase-8-positve apoptotic fiber cells in the "tail-like" tissue at P 15 days in dKO (Figure 3A). At P 30 days, caspase-8$^+$ apoptotic cells were primarily localized in the central and anterior regions of the lens, and CD68$^+$ macrophages were located inside the lens (Figure 3A). We further determined the relationship of macrophage and necrotic fiber cells by coimmunofluorescence staining with CD68 and RIP3 antibodies (Figure 3B). Similarly, RIP3$^+$ cells were detected at the lens fiber protrusion region of the posterior capsule, which coincided with the presence of CD68$^+$ macrophages. Moreover, inside the lens, macrophages were surrounded by RIP3$^+$ necrotic cells. These results suggest that macrophages are recruited by necrotic fiber cells, which are likely derived from caspase-8$^+$ apoptotic cells.

### Fibrosis activation in the posterior capsule-sealing process

By P 90 days, lens fiber tails had disappeared and the posterior capsule rupture had sealed in approximately 83% of lenses (Table 1B). To explore if capsular sealing was caused by increased fibrosis, immunostaining was performed with an antibody against, α-SMA, a fibrosis marker in dKO lens at P 30, 60, and 90 days. Increased fibrosis was detected after P 15 days. At P 30 days, α-SMA$^+$ fibrotic tissues were surrounded by the "tail-like" tissue. At P 90 days, the ruptured posterior capsule was fully repaired and thick fibrotic tissue was present throughout the posterior lens surface (Figure 4A). In addition, epithelial cells exhibited abnormal morphology, becoming nonpolarized and disorganized. Some epithelial cells were α-SMA positive, implying an epithelial mesenchymal transition (EMT) at P 30 days, which increased from P 30 to 90 days (arrows, Figure 4B). We used other EMT markers including E-cadherin and N-cadherin to further verify an EMT (Figure 4C). At P 30 days, the expression of E-cadherin decreased, whereas N-cadherin increased in the lens equatorial region of dKO lenses. Furthermore, the mRNA expression of fibronectin (Fn1), a fibrosis marker, was significantly increased in isolated dKO lens compared with WT, Cx50KO, and AQP0KO lenses at P 15 days (Figure 4D). In addition, the thickness of the anterior capsule was greatly increased at P 15 and 60 days and 12 months in the dKO lenses (arrows, Figure 4E). The quantification analysis showed that the thickness of anterior capsules was significantly elevated in dKO lenses compared with WT at P 60 days and 1 year (P 60 days, p = 0.0036; 1 year, p < 0.0001) (Figure S4). These results suggest that macrophage-associated EMT and fibrosis are directly involved in posterior capsule sealing and thickening of lens epithelial cells.

### M2 macrophages play a key role in capsular rupture sealing and fibrosis

Besides their location at the posterior ruptured lens region, macrophages were found in the anterior region of the lens adjacent to EMT cells in some dKOs (Figure 5A). M2 macrophages have been reported to be closely associated with fibrosis and EMT (Yao et al., 2018). Quantitative real-time reverse transcription polymerase chain reaction (RT-qPCR) data showed that mRNA levels of CD68 and the M2 macrophage marker, arginase 1 (Arg-1) were significantly elevated in dKO lenses compared with WT, Cx50KO, and AQP0KO lenses. M2 macrophages were detected at P 15 days (Figure 5B). The localization of subtypes of macrophages in the dKO lenses was analyzed using antibodies against CD68, nitric oxide synthase (iNOS), and Arg-1 to detect total, M1, and M2 macrophages, respectively (Figure 5C). M1 and M2 macrophages were detected in dKO lenses at P 15 days (Figure 5C, left two panels) and P 30 days (Figure 5C, right two panels). CD68$^+$ macrophages were localized in the "tail-like" tissue where they were colabeled with the
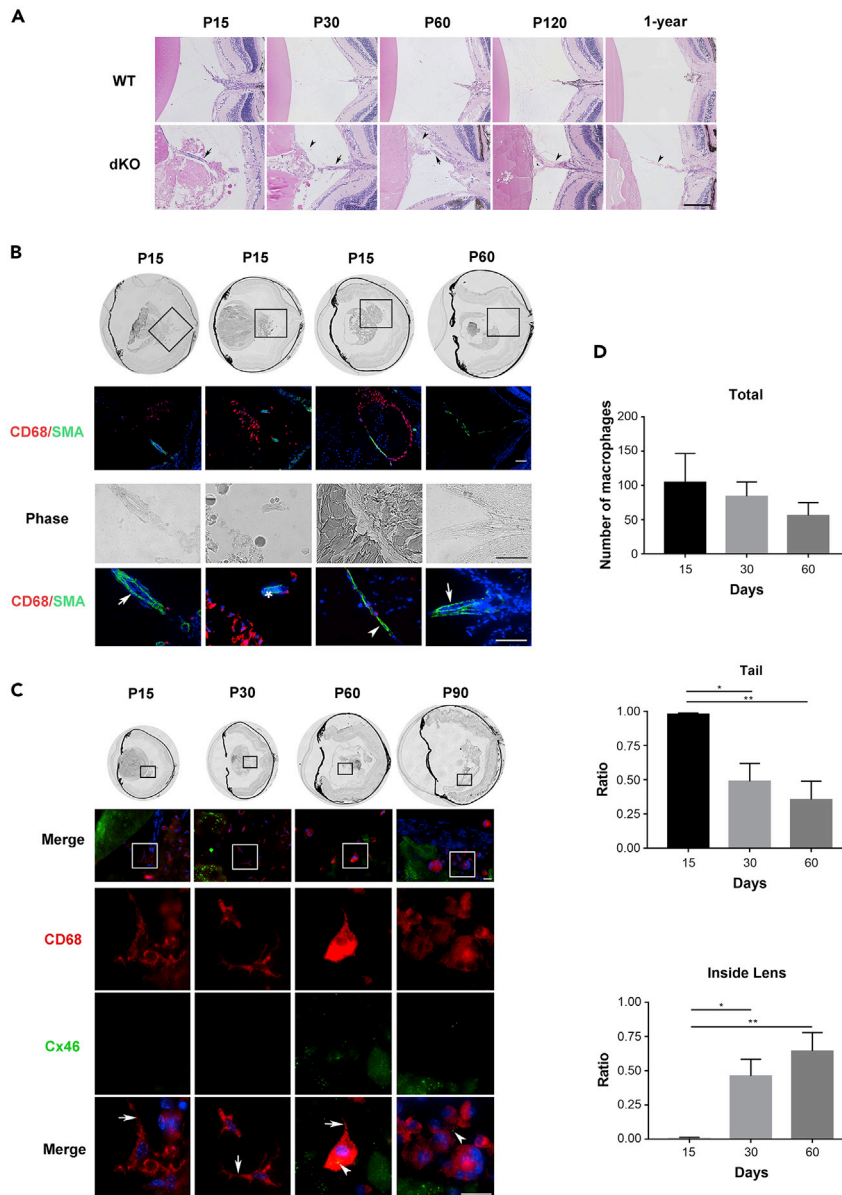
**Figure 2. Delayed regression of the hyaloid vessel system**

(A) Images of H&E-stained midsagittal paraffin lens sections from WT (upper panel) and dKO (lower panel) mice at ages of P 15, P 30, P 60 and P 120 days and P 1 year. dKO mouse retinal vasculature was connected to the lens posteriorly (black arrow) before P 60 days. Fibrotic tissues are indicated with black ars. Scale bar = 200 μm. n = 9–12/group.

(B) Cryosections of lens tissue of P 15 day and P 60 day dKO mice were immunostained with anti-CD68 antibody (red), α-SMA antibody (green), and counterstained with DAPI (blue). The hyaloid artery (HA) (white solid arrow); branches – the vasa hyaloidea propria (VHP, white asterisk); and tunica vasculosa lentis (TVL, white arrowhead) were labeled by α-SMA antibody (green fluorescence). Scale bar = 200 μm.

(C) Cryosections of the eyeball from dKO mice were coimmunostained with anti-CD68 antibody (red), Cx46 antibody (green), and counterstained with DPAI (blue) at P 15, P 30, P 60, and P 90 days. Pseudopodia of macrophages (solid white arrow) and lens fibers labeled by Cx46 antibody (solid white arrowhead) were shown. Scale bar = 20 μm.

(D) Total numbers (top panel) and number of macrophages at the tail region (middle panel) and inside the lens (bottom panel) at P 15, P 30, and P 60 days were quantified. *, p < 0.05, **, p < 0.01. All the data are presented as mean ± SEM. n = 5 per group.

M1 macrophage marker iNOS and M2 markers at P 15 days. However, most CD68^{+} macrophages inside the lens were colabeled with the M2 macrophage marker Arg-1 at P 30 days (Figure 5C). We quantified total, M1, and M2 macrophages in comparable tissue sections containing the HA at P 15 and 30 days. We found
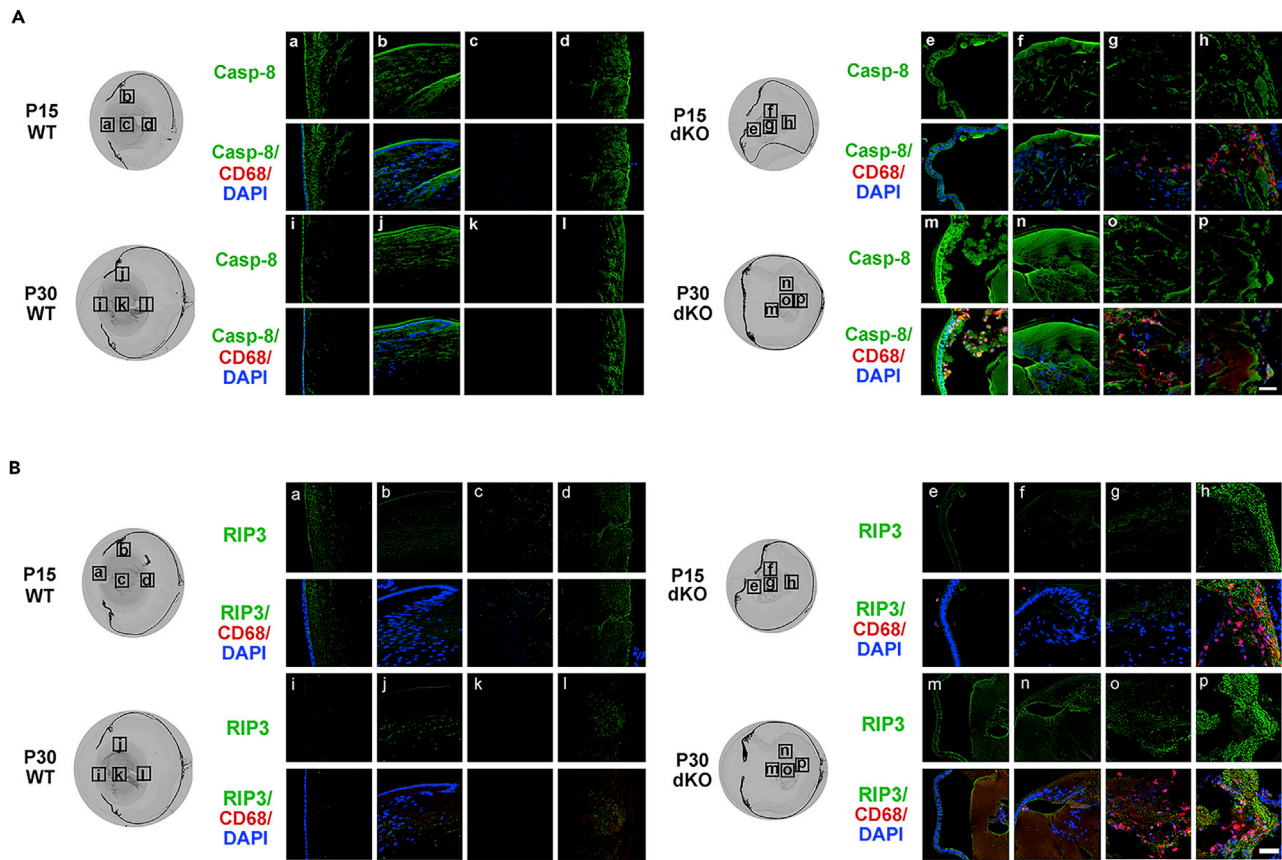
**Figure 3. Recruitment of macrophages by necrotic fiber cells**

Cryosections of eyeballs from WT and dKO mice were coimmunostained with anti-CD68 (red) and anti-caspase-8 antibodies (Casp-8, green, A) or RIP3 antibody (green, B). High-resolution fluorescence images of various regions of lenses at P 15 and P 30 days are indicated by frames on phase images on the corresponding left panels: anterior region (a, e, i, m), equator region (b, f, j, n), central region (c, g, k, o), and "tail-like" region (d, h, l, p). Scale bar = 50 μm.

that the number of CD68$^+$ macrophages in the "tail-like" tissue at P 30 days was significantly decreased as compared with that at P 15 days (p = 0.047). In contrast, compared with those in the P 15-day lens, the number of CD68$^+$ and Arg1$^+$ (M2) macrophages inside the P 30 days lens was significantly increased (p = 0.002 and p = 0.006, respectively) (Figure 5D). These data suggest that M1 macrophages that prevail at an early stage of a ruptured lens may aid in removal of dying fiber cells and polarize to M2 macrophages at a later stage inside the lens to promote fibrosis and capsular sealing.

RNA sequencing (RNA-seq) analysis was used to assess M2 macrophage markers in the isolated lenses of WT, Cx50KO, MIPKO and dKO mice at P 15 days. Continuous activation of M2 macrophages results in activation of fibroblasts through the release of transforming growth factor (TGF) -β, vascular endothelial growth factor A (VEGFA) and galectin-3 (GAL-3, LGALS3) (Lech and Anders, 2013; Lin et al., 2014; Pradere et al., 2013). The mRNA expression of TGFb1 (Figure S5A), VEGFA (Figure S5B), and LGALS3 (Figure S5C) was significantly increased in the lenses of the dKO compared with WT, Cx50KO, and AQP0KO at P 15 days. These results suggest that activation of M2 macrophages with elevated levels of TGF-β, VEGFA, and GAL-3 play key roles in tissue repair and fibrosis.

### Enhanced M2 macrophage polarization by CSF-1 accelerates posterior capsule sealing

CSF-1 is a hematopoietic growth factor known to promote proliferation, differentiation, and survival of monocytes and macrophages and M2 macrophage polarization (Stanley et al., 1997; Jones and Ricardo, 2013; Mia et al., 2014). Our RT-qPCR result showed that CSF-1 mRNA was expressed significantly higher in dKO mice than that in WT, Cx50KO, and AQP0 KOs at P 15 days (Figure 6A). To assess if increased M2 macrophages enhanced posterior capsule repair and fibrosis, CSF-1 was intravitreally injected in P
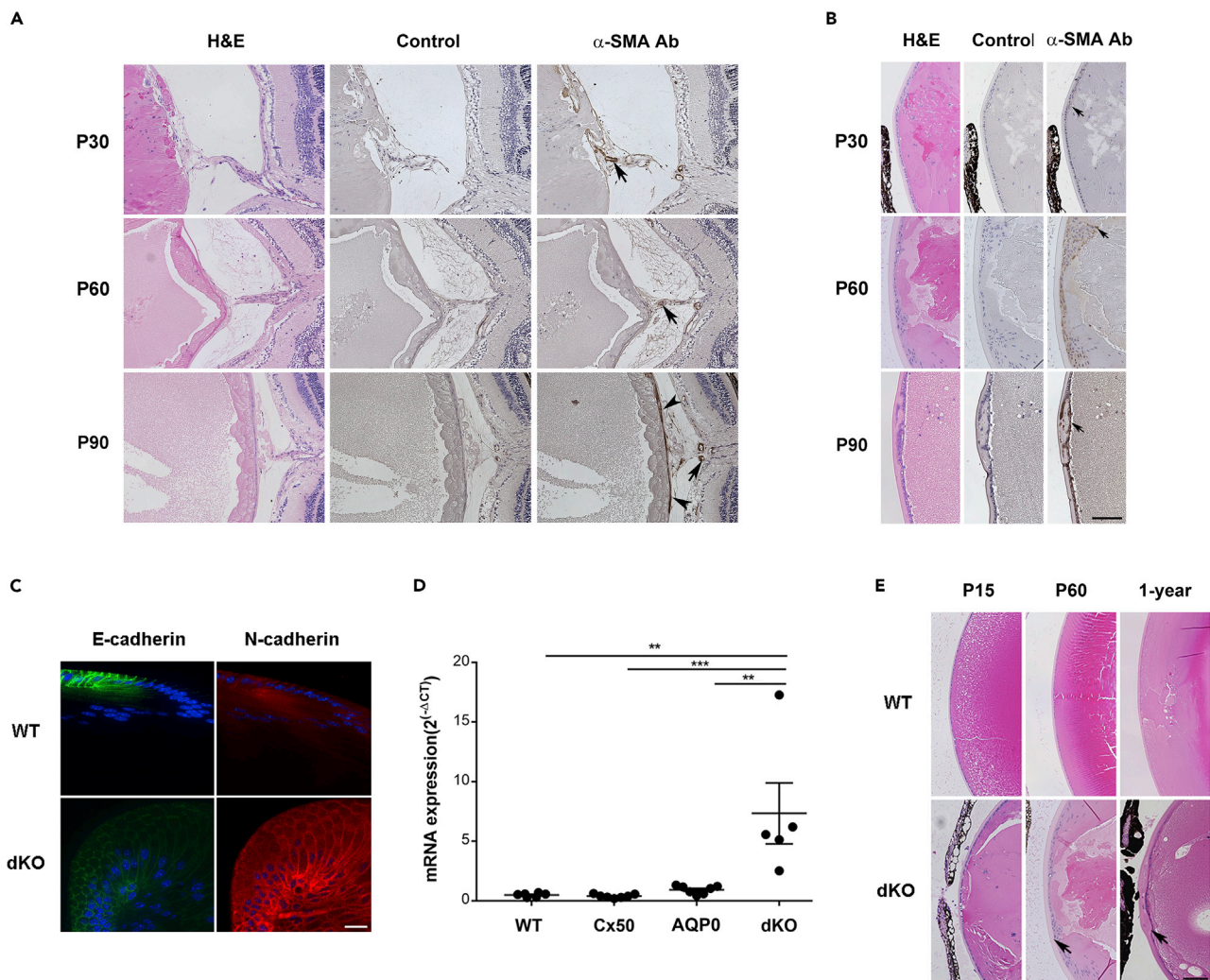
**Figure 4. Fibrosis formation is associated with repair of posterior capsule rupture and removal of the extruded "tail-like" tissue mass**

(A and B) (A) Posterior and (B) anterior of lens paraffin sections of eyeballs from dKO mice at P 30, P 60, and P 90 days were stained with H&E (left panel), negative control (middle panel), and anti-α-SMA antibody (right panels). Scale bar = 100 μm. A subset of activated fibrogenic cells and myofibroblasts is indicated in the posterior region of the lens (solid black ars) and around hyaloid vessel (solid black arrows) (A). The positive signals of α-SMA are indicated in anterior regions of the lens (solid black arrows) (B).

(C) Cryosections of the lenses from P 30 days dKO mice were immunofluorescence stained with anti-E-cadherin (green) or anti-N-cadherin (red) antibodies at equator regions. Bar = 20 μm.

(D) The mRNA expression of Fn-1 in WT, Cx50 KO, AQP0 KO and dKO lenses (WT, n = 6; Cx50 KO, n = 7; MIP KO n = 7; dKO, n = 5). **, p < 0.01; ***, p < 0.001.

(E) Midsagittal paraffin tissue sections of lenses from WT (upper panel) and dKO (lower panel) mice of P 15 days, 2 month, and 1 year of age were H&E stained and imaged at the anterior lens regions. The increased thickness of anterior capsule is indicated (solid black arrows) in dKO mice. Scale bar = 100 μm.

15-day dKO mice. A previous report shows that blood concentration of CSF-1 reaches 5–10 times higher 24 h after injection, and the numbers of macrophages also increase sharply within the same time frame (Hume and MacDonald, 2012). Immunostaining with anti-CD68, anti-iNOS and anti-Arg-1 antibodies showed the number of total macrophages and Arg-1^{+} M2 macrophages was markedly elevated 24 h after CSF-1 injection around the posterior lens region, while there was minimal increase of iNOS[+]-M1 micro-phages (Figure 6B). However, there was a significant increase of total and M2 macrophages in dKO mice 24 h after CSF-1 injection (Figure 6C). Moreover, the posterior lens capsules were completely sealed and replaced by fibrotic tissues (arrow, Figure 6D) earlier in CSF-1-injected than those in noninjected and saline-injected control P30 dKO mice (Figure 6D). In addition, increased thickness and EMT of lens epithelial cells were observed by α-SMA antibody staining (ars, Figure 6D). To further validate the specific effect of CSF-1, we used AFS98, a monoclonal antibody that blocks CSF-1 receptor function (Hume and
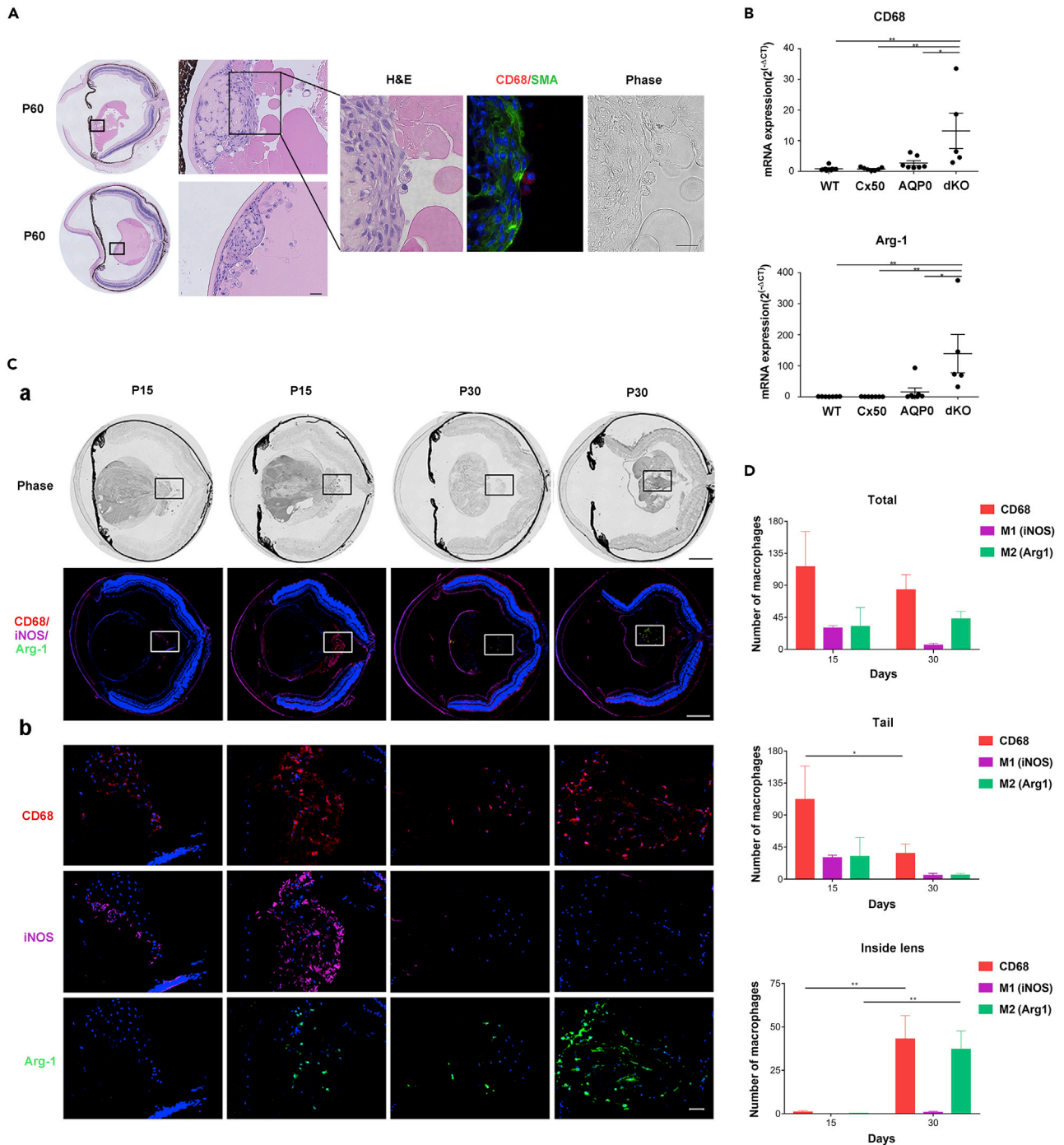
**Figure 5. Increased M2 and decreased M1 macrophages during posterior rupture repair**

(A) High-resolution images of midsagittal paraffin tissue sections of two examples of P 60-day dKO lenses. The lens regions are indicated in the black frames of lower magnification images on the left. Midsagittal paraffin tissue sections were coimmunostained with anti-CD68 and anti-α-SMA antibodies, macrophages were found around α-SMA-positive sites. Scale bar = 50 μm. (B) The mRNA expression of CD68 and Arg-1 in lenses of WT, Cx50 KO, MIP KO, and dKO at P 15 days (WT, n = 6; Cx50 KO, n = 7; MIP KO, n = 7; dKO n = 5) *, p < 0.05; **, p < 0.01.

(C) Cryosections of the whole eyeball from P 15-day and P 30-day dKO mice were immunostained with antibodies against macrophages (CD68^{+}, red), M1 (iNOS, purple), and M2 (Arg-1, green). Scale bar = 200 μm for low magnification (a) and scale bar = 20 μm for high magnification (b).

(D) The numbers of M1 and M2 macrophages in the entire lens, the ''tail-like'' regions, and inside lens at P 15 and 30 days were quantified. *, p < 0.05; **, p < 0.01; ***, p < 0.001; ****, p < 0.0001. n = 5 per group.
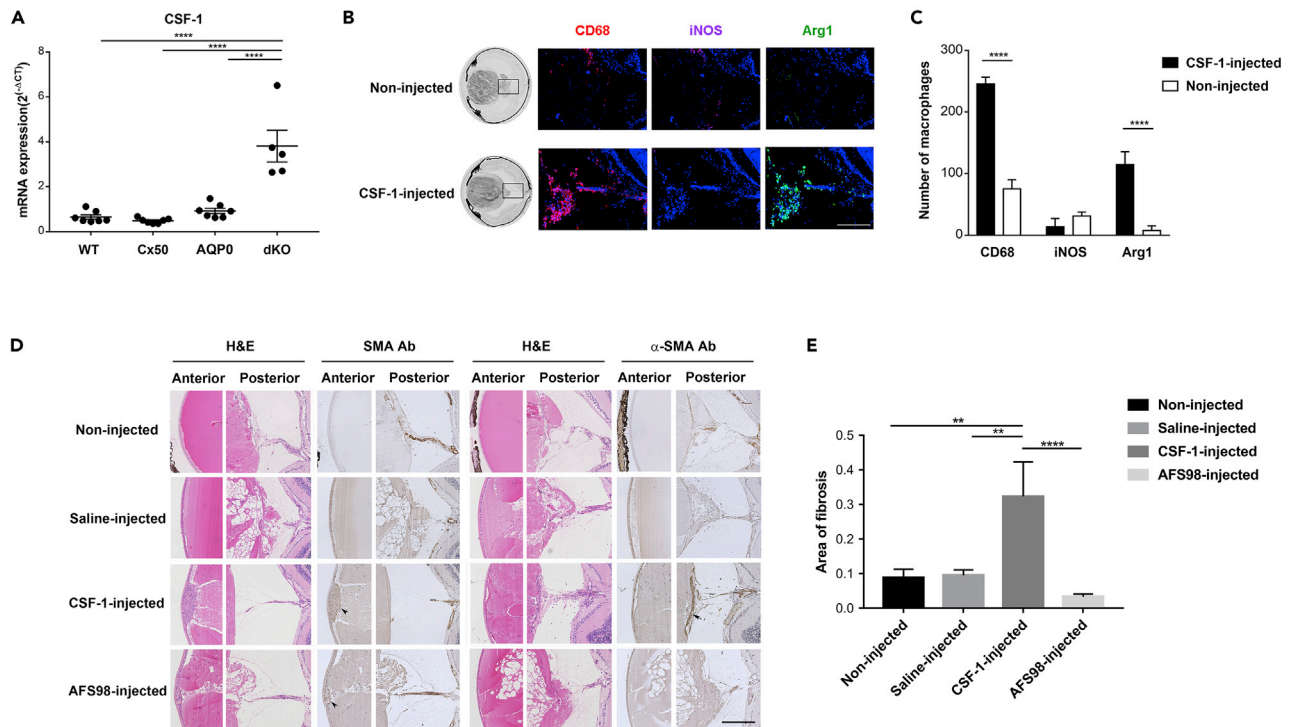
**Figure 6. Promotion of the "tail-like" tissue removal, posterior capsule repair, and polarization of M2 macrophages by CSF-1**

(A) The mRNA expression of CSF-1 was determined by RT-qPCR in WT, Cx50 KO, MIP KO, and dKO lenses at P 15 days (WT, n = 6; Cx50 KO, n = 7; MIP KO, n = 7; dKO, n = 5) *, p < 0.05; **, p < 0.01; ***, p < 0.001; ****, p < 0.0001.

(B) Cryosections of entire eyeballs from P 15 days dKO mice 24 h after CSF-1 injection were immunostained with CD68 (red), iNOS (purple), and Arg-1 (green). Scale bar = 200 μm.

(C) Total numbers (CD68$^+$), M1 (iNOS$^+$), and M2 (Arg-1$^+$) macrophages in the posterior regions were quantified 24 h after CSF-1 injection. All the data are presented as mean ± SD. n = 3 per group.

(D) Paraffin sections of four groups (noninjected, saline-injected, CSF-1-injected, and CSF-1 receptor inhibitor, AFS98-injected dKO mice at P 30 days were stained with H&E or anti-α-SMA antibody. EMT area (solid black ars) is indicated in anterior part of lens. A subset of activated fibrogenic cells and myofibroblasts (solid black arrow) is indicated in the posterior region. Scale bar = 200 μm.

(E) The fibrosis area in the posterior capsule in four groups, noninjected, n = 14; saline-injected, n = 17; CSF-1-injected, n = 8; AFS98-injected, n = 12.

MacDonald, 2012; Kubota et al., 2009). In contrast to CSF-1, AFS98 injection appeared to delay the sealing of the posterior lens capsule and removal of the "tail-like" tissue, although the thickness of epithelial cells remained similar (Figure 6D). The sealing rate of the posterior lens capsule rupture was greatly increased compared with the noninjected, saline-injected, and AFS98-injected groups (Table 3). The levels of fibrosis was assessed by α-SMA antibody staining in the lens posterior region of midsagittal tissue sections of the eyeball at P 30 days (Figure 6D). Fibrotic tissues were significantly increased in the CSF-1-injected group when compared with all other groups (Figure 6E), while fibrosis levels were reduced in the AFS98-injected group. These results suggest that polarization and formation of M2 macrophages by CSF-1 accelerate posterior lens capsular sealing and fibrosis.

## DISCUSSION

We have previously shown that dKO mice deficient in lens-specific Cx50 and AQP0 exhibit several lens defects. This is more evident in the posterior region of the lens, including posterior subcapsular and polar cataracts, and posterior capsular rupture with severe extrusion of lens fiber cells. We also reported disorganized fiber cell structures with abnormally enlarged extracellular spaces (Gu et al., 2019). By using this dKO mouse model, we report a direct mechanism for macrophages in the immune-privileged lens organ during damage repair and fibrosis. As illustrated in Figure 7, ruptured posterior capsules are associated with leaky "tail-like" lens fiber cells that delay the regression of hyaloid vessels and recruit macrophages to the lens. M1 macrophages delivered by hyaloid vessels appear to mediate the clearance of the "tail-like" fiber tissue mass outside the lens at the initial stage. At the later stage, the necrotic fiber cells promote

**Table 3. Outcome of injections**

| Injected | Repaired | No repaired |
|---|---|---|
| No (n = 15) | 1 | 14 |
| Saline (n = 18) | 1 | 17 |
| CSF-1 (n = 15) | 7 | 8 |
| AFS98 (n = 13) | 1 | 12 |

the polarization and transition to M2 macrophages inside the lens, leading to increased EMT, fibrosis, and posterior capsule rupture sealing. M2 macrophage activator, CSF-1 or a CSF-1 receptor inhibitor, accelerates or delays the sealing process and fibrosis, respectively.

Posterior capsular rupture is associated with cataract surgery, especially in patients with posterior opacification (Hua et al., 2018). Several clinical studies have shown that the incidence of posterior capsule rupture accounts for more than 30% of posterior polar cataract surgeries (Varadaraj et al., 1999; Das et al., 2008), which presents a big challenge for clinicians. Moreover, a ruptured capsule greatly increases the incidence of retinal detachment during and after surgery, resulting in serious clinical complications (Petousis et al., 2016). Several transgenic mouse models also show phenotypes of ruptured posterior capsules. In one study, lenses overexpressing acylpeptide hydrolase accumulate low-molecular-weight peptides and protein aggregates associated with increased posterior capsular rupture (Santhoshkumar et al., 2014). In a mouse model with lens deficiency of Rac 1 GTPase, lens morphological defects and posterior capsule ruptures have been previously described (Maddala et al., 2011). The posterior capsule ruptured phenotypes are also reported in mutant Lop10/Lop10 $\alpha3^{-/-}$ mice (Chang et al., 2002; Xia et al., 2006). In our dKO mouse model, the posterior capsule rupture is primarily attributed to a reduced cell-adhesion function with severe exacerbation of lens fiber cell organization and excessive enlargement of extracellular spaces as a result of Cx50/AQP0 deficiency in lens fibers (Hu et al., 2017; Gu et al., 2019). These severe disruptions of lens fiber structure are likely to generate extra physical stress on the thin, vulnerable posterior capsule, given the posterior capsule is thinner than that in other parts of the lens, and its thickness is decreased with aging (Barraquer et al., 2006; Krag and Andreassen, 2003).

We focused on the structure of the leaky, "tail-like" tissue mass in the vitreous cavity of the dKO, where both the un-regressed vessels and the macrophages along with the lens fiber tissue mass were identified. Associated with the growth of the eyeball, the vessels are derived from the hyaloid vessel system. The hyaloid vascular system, including the HA, the vasa hyaloidea propria (VHP), and the tunica vasculosa lentis (TVL), exists transiently during eye development. These structures provide nutrients in the early stage of lens development (Ito and Yoshioka, 1999; Jack, 1972; Zhu et al., 1999). In the WT mouse, the VHP and TVL start regressing after birth and disappear around P 15–16 days (Brown et al., 2005; Ito and Yoshioka, 1999; Kishimoto et al., 2018). Neonatal neurons that sequester VEGFA protein in the vitreous cavity is shown to cause endothelial apoptosis, which helps the regression of hyaloid vessels (Yoshikawa et al., 2016). It has also been reported that macrophages play a crucial role in the regression of the hyaloid vascular system (Kishimoto et al., 2018; Lang and Bishop, 1993). In dKO mice, the regression of the hyaloid vessel system is delayed and the number of macrophages is greatly increased in the vitreous cavity. It is intriguing how macrophages are generated and delivered to the posterior vitreous cavity. The anterior ciliary body of the eyeball has been reported to store and release macrophages in a lens-specific N-cadherin conditional KO mouse model (Logan et al., 2017). However, in our studies, we failed to detect any macrophages around the ciliary body at the early stage when macrophages are identified in the posterior vitreous cavity. We found the presence of macrophages inside or adjacent to the unrepressed hyaloid vessels amid the "tail-like" tissue. It is likely that factors possibly secreted by loose, abnormal lens cells extruded out of the ruptured capsule prevent the regression of hyaloid vessels. We did not observe the regrowth of the hyaloid vessels, probably because the capsule rupture occurs earlier during lens development in our models compared with others. The HA regresses after fibrotic closure of the posterior capsule. It is plausible that the release of VEGFA, likely induced by loosely extruded lens tissue, helps sustain hyaloid vessels to serve as a potential route to deliver macrophages to the vitreous cavity, the area closest to the posterior capsule rupture with the "tail-like" tissue mass. We observed that at the early stage, macrophages were surrounded by the extruded "tail-like" fiber cells, which were likely recruited by the increased number of necrotic fiber cells, possibly through cytokines released by necrotic cells (Chazaud, 2014). As expected, these necrotic
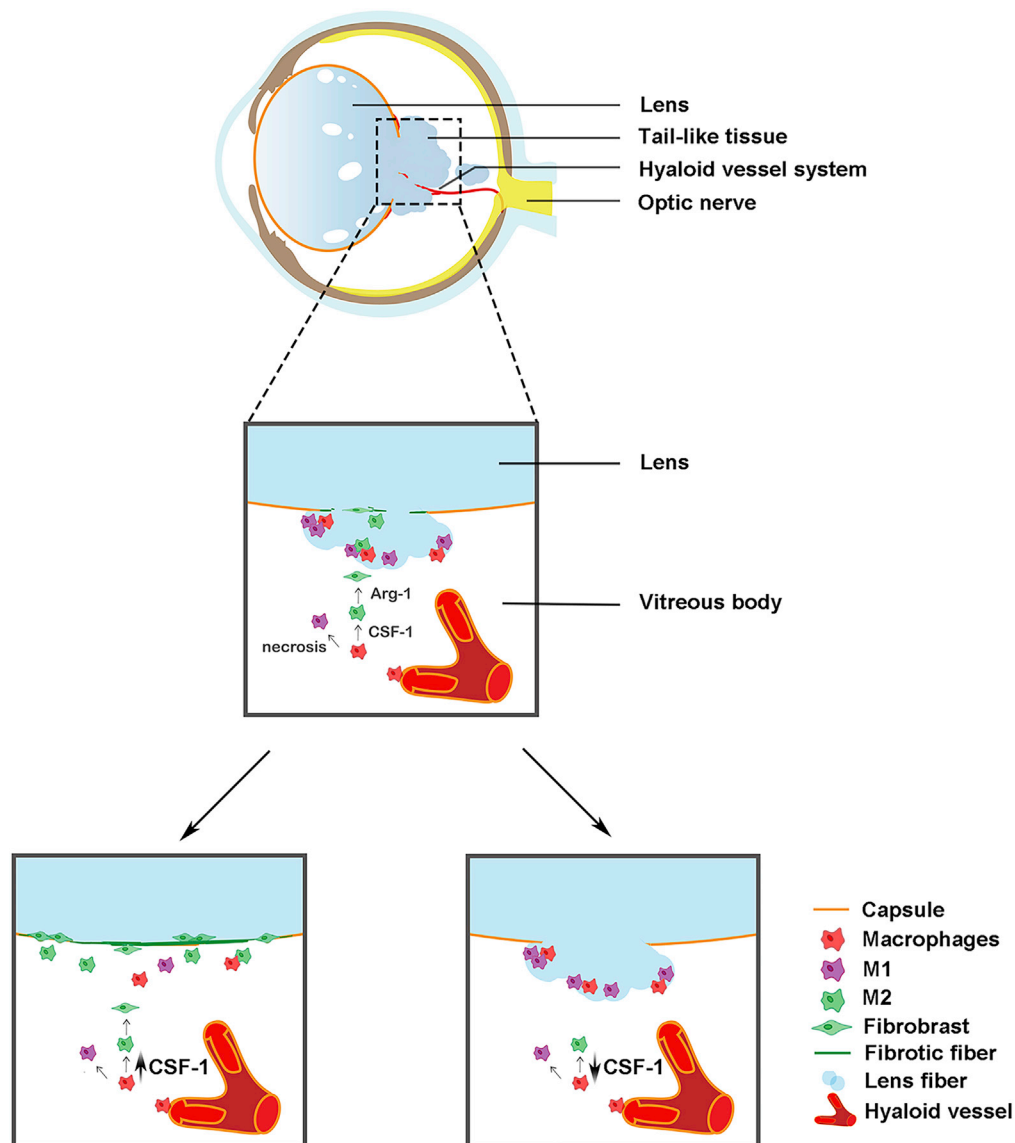
**Figure 7. Schematic diagram illustrating the role of macrophages in posterior capsule repair, lens fiber tissue mass removal and fibrosis**

In dKO mice, hyaloid vessels deliver macrophages to the vitreous cavity adjacent to the ruptured posterior capsule and the "tail-like" tissue mass. Necrotic tissues recruit microphages to the tissue mass, which mediates the removal of the tissue mass. CSF-1 promotes M2 macrophage polarization, posterior capsule sealing, and fibrosis (middle panel). Administration of CSF-1 accelerates the process of capsule repair, tissue removal, and fibrosis (lower left panel). Inhibition of CSF-1 receptor by administrating a blocking antibody delays the repair process (right lower panel).

lens fibers were associated with M2 macrophage and fiber cell markers, such as Cx46, which was detected inside the macrophages, indicating macrophage phagocytosis. During eye growth in the dKO, hyaloid vessels gradually regressed and the "tail-like" fiber tissue was removed. After clearance of fiber cells outside the lens, macrophages were detected inside the lens, possibly migrating through the ruptured posterior capsule.

The macrophages, primarily inside the lens, underwent polarization to M2 macrophages. M2 macrophages were identified not only in necrotic areas but also at sites with active fibrosis. We found a close correlation between areas with a large number of accumulated M2 macrophages and an increase in RIP3$^+$ necrotic fiber cells. A previous study has reported that Arg-1-expressing and ornithine-producing

M2 macrophages are necessary for tissue repair as opposed to NO-producing M1 macrophages, as the latter play a major role during the initial phase of inflammation observed during wound sealing (Albina et al., 1988, 1990; Rath et al., 2014). The M1 to M2 macrophage transition was recapitulated in our model. We found that at the early stage, around P 15 days, the CD68^{+}-macrophages were predominantly iNOS^{+} M1 macrophages intermingled with the "tail-like" fibers outside the lens, which implies the activation of the immune response. After removal of the fiber cells outside the lens after P 30 days, macrophages polarized to the M2 phenotype were associated with Arg-1 expression, which initiated the repair process and fibrosis.

Researchers found massive upregulation of known inflammatory mediators 24 h after cataract surgery in a mouse model (Jiang et al., 2018). Cataract surgery is a major trauma to the eye, which disrupts the homeostasis of corneal and anterior chamber, leading to a proinflammatory process by activation of immune cells. Unlike the anterior injury model, posterior capsule rupture is an intrinsic, localized event occurring in the posterior chamber. We found that macrophages were primarily activated and then differentiated into M2 macrophages, leading to fibrosis and the sealing of the posterior capsule. In addition, the macrophages recruited in posterior capsule rupture are delivered by delayed, regressed hyaloid vessels, not from the anterior chamber of the eye. However, we did not observe any increase of known inflammatory factors in the RNA-seq data obtained from dKO mouse eyes. Therefore, after posterior capsule rupture in dKO, macrophage activation, but not the increased proinflammatory responses, is likely to be responsible for capsule sealing and fibrosis.

TGF-β, which supports the polarization toward anti-inflammatory macrophages, induced tissue repair and fibrosis by activated VEGF-α and GAL-3 (Wynn and Vannella, 2016; Chujo et al., 2009). Of note, the release of TGF-β, VEGF-α, and GAL-3, which play key roles in tissue repair and fibrosis, increased significantly at P 15 days in dKO. This is mainly caused by continuous activation of M2 macrophages that lead to activation of fibroblasts through the release of TGF-β, VEGF-α, and galectin-3 (Lech and Anders, 2013; Lin et al., 2014; Pradere et al., 2013). On the one hand, TGF-β induced immune cells to produce VEGF-α, which will help delay the haloid vessels regression to deliver macrophages. On the other hand, GAL-3 is secreted by macrophages, and its expression is intimately connected with enhancing fibrosis-related factor expression in fibroblasts (Lin et al., 2014; Liu et al., 1995). It is accepted that fibroblast/myofibroblast transition starts with the appearance of the protomyofibroblast and followed by the differentiated myofibroblast with stress fibers containing SMA. Myofibroblast differentiation is regulated by TGF-1. The myofibroblast is a critical cell for the connective tissue remodeling that takes place during wound sealing and fibrosis development by producing cellular fibronectin (Duffield et al., 2005; Gabbiani, 2003). Therefore, activation of M2 macrophages induces the TGF-β, VEGF-α, and GAL-3 expression, which may aid in the sealing of the posterior capsule by promoting fibrosis in our mouse model.

Anterior lens capsule is primarily composed of laminin, collagen IV, and sulfated glycosaminoglycans (Ronci et al., 2011). The basement membrane functions as a molecular sieve, adjusting the transport of nutrients, metabolites, and signaling molecules (Danysh et al., 2010). We observed posterior capsule sealing by fibrosis. Meanwhile, we found that the anterior area is positive for SMA, indicating an EMT process. EMT is also known to have elevated type I collagen and fibronectin (Hay and Zuk, 1995). Here, we used several markers, SMA, N-cadherin, and E-cadherin to confirm EMT and fibrosis. Therefore, M1 macrophages are predominantly present outside the lens at the early stage, likely playing a role in removing the "tail-like" tissue mass, whereas M2 macrophages at the later stage mediate capsule rupture repair and fibrosis.

We identified that CSF-1 is a major factor in M2 macrophage polarization and fibrosis activation in the repair process. M2 macrophages have shown to limit tissue damage caused by inflammatory processes and stimulate tissue repair and remodeling (Mosser and Edwards, 2008). To test the hypothesis that the promotion of M2 macrophages by CSF-1 accelerates posterior capsule repair and fibrosis, we delivered CSF-1 into the posterior vitreous cavity using intravitreal injection. Indeed, posterior capsule repair occurred earlier in CSF-1-injected mice along with increased fibrotic tissue after more M2 macrophages were activated. The role of CSF-1 was further verified by a blocking antibody AFS98, by which inhibition of CSF-1 receptor function delayed capsule repair and reduced fibrosis. Excessive M2 macrophage activation is reported to result in promoting proliferation of myofibroblasts and inducing EMT (Braga et al., 2015; Conway and Hughes, 2012). In our model, after P 30 days and with aggravation of fibrosis, the

posterior capsule thickness increased, and EMT was initiated in lens epithelial cells. Based on these evidences, we believe that in addition to EMT of lens cells, altered morphology could be attributed by the involvement of multiple cell types including M2 macrophages and possibly fibroblasts. In summary, macrophages, as a major component of the immune system, plays key roles in damage repair, tissue removal and fibrosis in the immune-privileged lens organ, and these functions depend on M1 and M2 macrophages, respectively.

### Limitations of the study

We acknowledge certain limitation in our study. In this study, we used a dKO mouse model with a posterior capsule rupture. We have not identified and compared with other animal models with similar phenotypes.

### STAR★METHODS

Detailed methods are provided in the online version of this paper and include the following:

- KEY RESOURCES TABLE
- RESOURCE AVAILABILITY
  - Lead contact
  - Materials availability
  - Data and code availability
- EXPERIMENTAL MODEL AND SUBJECT DETAILS
  - dKO mice deficient of both Cx50 and AQP0
- METHOD DETAILS
  - Materials
  - Measurements of eye size and lens weight
  - Tissue paraffin sections and hematoxylin and eosin staining
  - Frozen lens tissue sections and fluorescence microscopy
  - Immunohistochemistry staining
  - Isolation of RNA from lens tissues and RT-qPCR
  - Intravitreal injection
  - Measure the number of macrophages and thickness of anterior capsule
- QUANTIFICATION AND STATISTICAL ANALYSIS

### AUTHOR CONTRIBUTIONS

Jean X. Jiang designed the study; Yuting Li and Sumin Gu conducted studies and performed experiments; Yuting Li and Zhen Li processed samples; Yuting Li and Yumeng Quan performed statistical analysis; Yuting Li and Jean X. Jiang wrote the manuscript; Hongyun Cheng managed and supplied experimental animals; Manuel A. Riquelme and Xiao-Dong Li provided suggestions and helped design the study; all authors critically revised and approved the manuscript.

### DECLARATION OF INTERESTS

The authors declare no competing interests.

## REFERENCES

Al-Ghoul, K.J., Kirk, T., Kuszak, A.J., Zoltoski, R.K., Shiels, A., and Kuszak, J.R. (2003). Lens structure in MIP-deficient mice. Anat. Rec. A. Discov. Mol. Cell Evol. Biol. *273*, 714–730.

Albina, J.E., Mills, C.D., Barbul, A., Thirkill, C.E., Henry, W.L.,, JR., Mastrofrancesco, B., and Caldwell, M.D. (1988). Arginine metabolism in wounds. Am. J. Physiol. *254*, E459–E467.

Albina, J.E., Mills, C.D., Henry, W.L., Jr., and Caldwell, M.D. (1990). Temporal expression of different pathways of 1-arginine metabolism in healing wounds. J. Immunol. *144*, 3877–3880.

Barraquer, R.I., Michael, R., Abreu, R., Lamarca, J., and Tresserra, F. (2006). Human lens capsule thickness as a function of age and location along the sagittal lens perimeter. Invest. Ophthalmol. Vis. Sci. *47*, 2053–2060.

Braga, T.T., Agudelo, J.S., and Camara, N.O. (2015). Macrophages during the fibrotic process: M2 as friend and foe. Front. Immunol. *6*, 602.

Brown, A.S., Leamen, L., Cucevic, V., and Foster, F.S. (2005). Quantitation of hemodynamic function during developmental vascular regression in the mouse eye. Invest. Ophthalmol. Vis. Sci. *46*, 2231–2237.

Chang, B., Wang, X., Hawes, N.L., Ojakian, R., Davisson, M.T., Lo, W.K., and Gong, X. (2002). A Gja8 (Cx50) point mutation causes an alteration of alpha 3 connexin (Cx46) in semi-dominant cataracts of Lop10 mice. Hum. Mol. Genet. *11*, 507–513.

Chazaud, B. (2014). Macrophages: supportive cells for tissue repair and regeneration. Immunobiology *219*, 172–178.

Chepelinsky, A.B. (2009). Structural function of MIP/aquaporin 0 in the eye lens; genetic defects lead to congenital inherited cataracts. Handb Exp. Pharmacol. *190*, 265–297.

Chujo, S., Shirasaki, F., Kondo-Miyazaki, M., Ikawa, Y., and Takehara, K. (2009). Role of connective tissue growth factor and its interaction with basic fibroblast growth factor and macrophage chemoattractant protein-1 in skin fibrosis. J. Cell Physiol. *220*, 189–195.

Conway, B., and Hughes, J. (2012). Cellular orchestrators of renal fibrosis. Q.J.M. *105*, 611–615.

Danysh, B.P., Patel, T.P., Czymmek, K.J., Edwards, D.A., Wang, L., Pande, J., and Duncan, M.K. (2010). Characterizing molecular diffusion in the lens capsule. Matrix Biol. *29*, 228–236.

Das, S., Khanna, R., Mohiuddin, S.M., and Ramamurthy, B. (2008). Surgical and visual outcomes for posterior polar cataract. Br. J. Ophthalmol. *92*, 1476–1478.

Duffield, J.S., Forbes, S.J., Constandinou, C.M., Clay, S., Partolina, M., Vuthoori, S., Wu, S., Lang, R., and Iredale, J.P. (2005). Selective depletion of macrophages reveals distinct, opposing roles during liver injury and repair. J. Clin. Invest. *115*, 56–65.

Gabbiani, G. (2003). The myofibroblast in wound healing and fibrocontractive diseases. J. Pathol. *200*, 500–503.

Gerhardt, H., Golding, M., Fruttiger, M., Ruhrberg, C., Lundkvist, A., Abramsson, A., Jeltsch, M., Mitchell, C., Alitalo, K., Shima, D., and Betsholtz, C. (2003). VEGF guides angiogenic sprouting utilizing endothelial tip cell filopodia. J. Cell Biol. *161*, 1163–1177.

Godwin, J.W., and Brockes, J.P. (2006). Regeneration, tissue injury and the immune response. J. Anat. *209*, 423–432.

Gong, X., Li, E., Klier, G., Huang, Q., Wu, Y., Lei, H., Kumar, N.M., Horwitz, J., and Gilula, N.B. (1997). Disruption of alpha3 connexin gene leads to proteolysis and cataractogenesis in mice. Cell *91*, 833–843.

Gratchev, A., Kzhyshkowska, J., Kothe, K., Muller-Molinet, I., Kannookadan, S., Utikal, J., and Goerdt, S. (2006). Mphi1 and Mphi2 can be re-polarized by Th2 or Th1 cytokines, respectively, and respond to exogenous danger signals. Immunobiology *211*, 473–486.

Gu, S., Biswas, S., Rodriguez, L., Li, Z., Li, Y., Riquelme, M.A., Shi, W., Wang, K., White, T.W., Reilly, M., et al. (2019). Connexin 50 and AQP0 are essential in maintaining organization and integrity of lens fibers. Invest. Ophthalmol. Vis. Sci. *60*, 4021–4032.

Hay, E.D., and Zuk, A. (1995). Transformations between epithelium and mesenchyme: normal, pathological, and experimentally induced. Am. J. Kidney Dis. *26*, 678–690.

Hu, Z., Shi, W., Riquelme, M.A., Shi, Q., Biswas, S., Lo, W.K., White, T.W., Gu, S., and Jiang, J.X. (2017). Connexin 50 functions as an adhesive molecule and promotes lens cell differentiation. Sci. Rep. *7*, 5298.

Hua, X., Dong, Y., Du, J., Yang, J., and Yuan, X. (2018). Phacoemulsification with hydrodelineation and OVD-assisted hydrodissection in posterior polar cataract. BMC Ophthalmol. *18*, 165.

Hume, D.A., and MacDonald, K.P. (2012). Therapeutic applications of macrophage colony-stimulating factor-1 (CSF-1) and antagonists of CSF-1 receptor (CSF-1R) signaling. Blood *119*, 1810–1820.

Ito, M., and Yoshioka, M. (1999). Regression of the hyaloid vessels and pupillary membrane of the mouse. Anat. Embryol. (Berl) *200*, 403–411.

Jack, R.L. (1972). Ultrastructural aspects of hyaloid vessel development. Arch. Ophthalmol. *87*, 427–437.

Jiang, J., Shihan, M.H., Wang, Y., and Duncan, M.K. (2018). Lens epithelial cells initiate an inflammatory response following cataract surgery. Invest. Ophthalmol. Vis. Sci. *59*, 4986–4997.

Jiang, J.X. (2010). Gap junctions or hemichannel-dependent and independent roles of connexins in cataractogenesis and lens development. Curr. Mol. Med. *10*, 851–863.

Jones, C.V., and Ricardo, S.D. (2013). Macrophages and CSF-1: implications for development and beyond. Organogenesis *9*, 249–260.

Kishimoto, A., Kimura, S., Nio-Kobayashi, J., Takahashi-Iwanaga, H., Park, A.M., and Iwanaga, T. (2018). Histochemical characteristics of regressing vessels in the hyaloid vascular system of neonatal mice: novel implication for vascular atrophy. Exp. Eye Res. *172*, 1–9.

Kistler, J., Kirkland, B., and Bullivant, S. (1985). Identification of a 70,000-D protein in lens membrane junctional domains. J. Cell Biol. *101*, 28–35.

Krag, S., and Andreassen, T.T. (2003). Mechanical properties of the human posterior lens capsule. Invest. Ophthalmol. Vis. Sci. *44*, 691–696.

Kubota, Y., Takubo, K., Shimizu, T., Ohno, H., Kishi, K., Shibuya, M., Saya, H., and Suda, T. (2009). M-CSF inhibition selectively targets pathological angiogenesis and lymphangiogenesis. J. Exp. Med. *206*, 1089–1102.

Kumari, S.S., Eswaramoorthy, S., Mathias, R.T., and Varadaraj, K. (2011). Unique and analogous functions of aquaporin 0 for fiber cell architecture and ocular lens transparency. Biochim. Biophys. Acta *1812*, 1089–1097.

Lang, R.A., and Bishop, J.M. (1993). Macrophages are required for cell death and tissue remodeling in the developing mouse eye. Cell *74*, 453–462.

Lech, M., and Anders, H.J. (2013). Macrophages and fibrosis: how resident and infiltrating mononuclear phagocytes orchestrate all phases of tissue injury and repair. Biochim. Biophys. Acta *1832*, 989–997.

Lee, E.J., Rosenbaum, J.T., and Planck, S.R. (2010). Epifluorescence intravital microscopy of murine corneal dendritic cells. Invest. Ophthalmol. Vis. Sci. *51*, 2101–2108.

Lin, Y.H., Chou, C.H., Wu, X.M., Chang, Y.Y., Hung, C.S., Chen, Y.H., Tzeng, Y.L., WU, V.C., HO, Y.L., HSIEH, F.J., et al. (2014). Aldosterone induced galectin-3 secretion in vitro and in vivo: from cells to humans. PLoS One *9*, e95254.

Liu, F.T., Hsu, D.K., Zuberi, R.I., Kuwabara, I., Chi, E.Y., and Henderson, W.R., Jr. (1995). Expression and function of galectin-3, a beta-galactoside-binding lectin, in human monocytes and macrophages. Am. J. Pathol. *147*, 1016–1028.

Liu, J., Xu, J., Gu, S., Nicholson, B.J., and Jiang, J.X. (2011). Aquaporin 0 enhances gap junction coupling via its cell adhesion function and interaction with connexin 50. J. Cell Sci. *124*, 198–206.

Lo, W.K., Biswas, S.K., Brako, L., Shiels, A., Gu, S., and Jiang, J.X. (2014). Aquaporin-0 targets interlocking domains to control the integrity and transparency of the eye lens. Invest. Ophthalmol. Vis. Sci. *55*, 1202–1212.

Logan, C.M., Bowen, C.J., and Menko, A.S. (2017). Induction of immune surveillance of the dysmorphogenic lens. Sci. Rep. *7*, 16235.

Maddala, R., Chauhan, B.K., Walker, C., Zheng, Y., Robinson, M.L., Lang, R.A., and Rao, P.V. (2011). Rac1 GTPase-deficient mouse lens exhibits defects in shape, suture formation, fiber cell migration and survival. Dev. Biol. *360*, 30–43.

Martinez, F.O., Sica, A., Mantovani, A., and Locati, M. (2008). Macrophage activation and polarization. Front. Biosci. *13*, 453–461.

Mathias, J.R., Dodd, M.E., Walters, K.B., Yoo, S.K., Ranheim, E.A., and Huttenlocher, A. (2009). Characterization of zebrafish larval inflammatory macrophages. Dev. Comp. Immunol. *33*, 1212–1217.

Medawar, P.B. (1948). Immunity to homologous grafted skin; the fate of skin homografts transplanted to the brain, to subcutaneous tissue, and to the anterior chamber of the eye. Br. J. Exp. Pathol. *29*, 58–69.

Mia, S., Warnecke, A., Zhang, X.M., Malmstrom, V., and Harris, R.A. (2014). An optimized protocol for human M2 macrophages using M-CSF and IL-4/IL-10/TGF-beta yields a dominant immunosuppressive phenotype. Scand. J. Immunol. *79*, 305–314.

Moriwaki, K., and Chan, F.K. (2013). RIP3: a molecular switch for necrosis and inflammation. Genes Dev. *27*, 1640–1649.

Mosser, D.M., and Edwards, J.P. (2008). Exploring the full spectrum of macrophage activation. Nat. Rev. Immunol. *8*, 958–969.

Pal-Ghosh, S., Pajoohesh-Ganji, A., Menko, A.S., Oh, H.Y., Tadvalkar, G., Saban, D.R., and Stepp, M.A. (2014). Cytokine deposition alters leukocyte morphology and initial recruitment of monocytes and gammadeltaT cells after corneal injury. Invest. Ophthalmol. Vis. Sci. *55*, 2757–2765.

Paul, D.L., Ebihara, L., Takemoto, L.J., Swenson, K.I., and Goodenough, D.A. (1991). Connexin46, a novel lens gap junction protein, induces voltage-gated currents in nonjunctional plasma membrane of Xenopus oocytes. J. Cell Biol. *115*, 1077–1089.

Petousis, V., Sallam, A.A., Haynes, R.J., Patel, C.K., Tyagi, A.K., Kirkpatrick, J.N., and Johnston, R.L. (2016). Risk factors for retinal detachment following cataract surgery: the impact of posterior capsular rupture. Br. J. Ophthalmol. *100*, 1461–1465.

Pradere, J.P., Kluwe, J., de Minicis, S., Jiao, J.J., Gwak, G.Y., Dapito, D.H., Jang, M.K., Guenther, N.D., Mederacke, I., Friedman, R., et al. (2013). Hepatic macrophages but not dendritic cells contribute to liver fibrosis by promoting the survival of activated hepatic stellate cells in mice. Hepatology *58*, 1461–1473.

Rath, M., Muller, I., Kropf, P., Closs, E.I., and Munder, M. (2014). Metabolism via arginase or nitric oxide synthase: two competing arginine pathways in macrophages. Front. Immunol. *5*, 532.

Ronci, M., Sharma, S., Chataway, T., Burdon, K.P., Martin, S., Craig, J.E., and Voelcker, N.H. (2011). MALDI-MS-imaging of whole human lens capsule. J. Proteome Res. *10*, 3522–3529.

Santhoshkumar, P., Xie, L., Raju, M., Reneker, L., and Sharma, K.K. (2014). Lens crystallin modifications and cataract in transgenic mice overexpressing acylpeptide hydrolase. J. Biol. Chem. *289*, 9039–9052.

Shechter, R., London, A., and Schwartz, M. (2013). Orchestrated leukocyte recruitment to immune-privileged sites: absolute barriers versus educational gates. Nat. Rev. Immunol. *13*, 206–218.

Sica, A., and Mantovani, A. (2012). Macrophage plasticity and polarization: in vivo veritas. J. Clin. Invest. *122*, 787–795.

Sonoda, K.H., Sakamoto, T., Qiao, H., Hisatomi, T., Oshima, T., Tsutsumi-Miyahara, C., Exley, M., Balk, S.P., Taniguchi, M., and Ishibashi, T. (2005). The analysis of systemic tolerance elicited by antigen inoculation into the vitreous cavity: vitreous cavity-associated immune deviation. Immunology *116*, 390–399.

Stanley, E.R., Berg, K.L., Einstein, D.B., Lee, P.S., Pixley, F.J., Wang, Y., and Yeung, Y.G. (1997). Biology and action of colony–stimulating factor-1. Mol. Reprod. Dev. *46*, 4–10.

Streilein, J.W. (2003). Ocular immune privilege: therapeutic opportunities from an experiment of nature. Nat. Rev. Immunol. *3*, 879–889.

Sun, X., Lee, J., Navas, T., Baldwin, D.T., Stewart, T.A., and Dixit, V.M. (1999). RIP3, a novel apoptosis-inducing kinase. J. Biol. Chem. *274*, 16871–16875.

Taylor, A.W., and Kaplan, H.J. (2010). Ocular immune privilege in the year 2010: ocular immune privilege and uveitis. Ocul. Immunol. Inflamm. *18*, 488–492.

Varadaraj, K., Kushmerick, C., Baldo, G.J., Bassnett, S., Shiels, A., and Mathias, R.T. (1999). The role of MIP in lens fiber cell membrane transport. J. Membr. Biol. *170*, 191–203.

White, T.W., Bruzzone, R., Goodenough, D.A., and Paul, D.L. (1992). Mouse Cx50, a functional member of the connexin family of gap junction proteins, is the lens fiber protein MP70. Mol. Biol. Cell *3*, 711–720.

White, T.W., Goodenough, D.A., and Paul, D.L. (1998). Targeted ablation of connexin50 in mice results in microphthalmia and zonular pulverulent cataracts. J. Cell Biol. *143*, 815–825.

Wynn, T.A., and Vannella, K.M. (2016). Macrophages in tissue repair, regeneration, and fibrosis. Immunity *44*, 450–462.

Xia, C.H., Liu, H., Cheung, D., Cheng, C., Wang, E., Du, X., Beutler, B., Lo, W.K., and Gong, X. (2006). Diverse gap junctions modulate distinct mechanisms for fiber cell formation during lens development and cataractogenesis. Development *133*, 2033–2040.

Yao, R.R., Li, J.H., Zhang, R., Chen, R.X., and Wang, Y.H. (2018). M2-polarized tumor-associated macrophages facilitated migration and epithelial-mesenchymal transition of HCC cells via the TLR4/STAT3 signaling pathway. World J. Surg. Oncol. *16*, 9.

Yin, X., Gu, S., and Jiang, J.X. (2001). Regulation of lens connexin 45.6 by apoptotic protease, caspase-3. Cell Commun. Adhes *8*, 373–376.

Yin, X., Liu, J., and Jiang, J.X. (2008). Lens fiber connexin turnover and caspase-3-mediated cleavage are regulated alternately by phosphorylation. Cell Commun. Adhes *15*, 1–11.

Yoshikawa, Y., Yamada, T., Tai-Nagara, I., Okabe, K., Kitagawa, Y., Ema, M., and Kubota, Y. (2016). Developmental regression of hyaloid vasculature is triggered by neurons. J. Exp. Med. *213*, 1175–1183.

Yu, X.S., and Jiang, J.X. (2004). Interaction of major intrinsic protein (aquaporin-0) with fiber connexins in lens development. J. Cell Sci. *117*, 871–880.

Yu, X.S., Yin, X., Lafer, E.M., and Jiang, J.X. (2005). Developmental regulation of the direct interaction between the intracellular loop of connexin 45.6 and the C terminus of major intrinsic protein (aquaporin-0). J. Biol. Chem. *280*, 22081–22090.

Zandy, A.J., Lakhani, S., Zheng, T., Flavell, R.A., and Bassnett, S. (2005). Role of the executioner caspases during lens development. J. Biol. Chem. *280*, 30263–30272.

Zhang, D.W., Shao, J., Lin, J., Zhang, N., Lu, B.J., Lin, S.C., Dong, M.Q., and Han, J. (2009). RIP3, an energy metabolism regulator that switches TNF-induced cell death from apoptosis to necrosis. Science *325*, 332–336.

Zhu, M., Provis, J.M., and Penfold, P.L. (1999). The human hyaloid system: cellular phenotypes and inter-relationships. Exp. Eye Res. *68*, 553–563.

## STAR★METHODS

### KEY RESOURCES TABLE

| REAGENT or RESOURCE | SOURCE | IDENTIFIER |
|---|---|---|
| **Antibodies** | | |
| Rat anti-mouse CD68 polyclonal antibody | BIO-RAD (Hercules, CA, USA) | Cat# MCA1957; RRID:AB_322219 |
| Monoclonal mouse anti-human smooth muscle actin antibody | Agilent (Santa Clara, CA, USA) | Cat# M085129-2; RRID:AB_2811108 |
| Goat anti-connexin 46 polyclonal antibody | Santa Cruz (Dallas, TX, USA) | Cat# sc-20861; RRID: AB_2110334 |
| Rabbit cleaved caspase-3 antibody | Fisher Scientific (Pittsburgh, PA, USA) | Cat# AP3725a; RRID: AB_10665003 |
| Rabbit cleaved caspase-8 antibody | Novus Biologicals (CO, USA) | Cat# NB100-56116; RRID: AB_837874 |
| Rabbit RIPK3/RIP3 antibody | Novus Biologicals (CO, USA) | Cat# NBP1-77299; RRID: AB_11040928 |
| Rabbit iNOS polyclonal antibody | Novus Biologicals (CO, USA) | Cat# NB100-59740; RRID: AB_892299 |
| Anti-mouse CSF1R (AFS98) monoclonal antibody | Fisher Scientific (Pittsburgh, PA, USA) | Cat# BE0213; RRID: AB_2687699 |
| **Chemicals, peptides, and recombinant proteins** | | |
| CSF-1 (mouse) recombinant protein | Abnova (Taipei, Taiwan) | P4588 |
| **Experimental models: Organisms/strains** | | |
| Cx50 and AQP0 double knockout (Cx50$^{-/-}$/Aqp0$^{-/-}$) mouse; C57BL/6 | Gu et al., 2019 | University of Texas Health Science center at San Antonio |
| Cx50 knockout (Cx50$^{-/-}$) mouse; C57BL/6 | White et al., 1998 | Stony Brook University |
| AQP0 knockout (Aqp$^{-/-}$)mouse | Alan Shiels et al., 2001 | Washington University School of Medicine |
| **Oligonucleotides** | | |
| Primer: CD68 Forward: CCCACCTGTCTCTCTCATTTC | This article | N/A |
| Primer: CD68 Reverse: GTATTCCACCGCCATGTAGT | This article | N/A |
| Primer: CSF-1 Forward: CAGGTGGAACTGCCAGTATAG | This article | N/A |
| Primer: CSF-1 Reverse: GAAGATGGTAGGAGAGGGTAGT | This article | N/A |
| Primer: Arg-1 Forward: CAGAGGTCCAGAAGAATGGAAG | This article | N/A |
| Primer: Arg-1 Reverse: TCCACCCAAATGACACATAGG | This article | N/A |
| Primer: Fn-1 Forward: TCCTGTCTACCTCACAGACTAC | This article | N/A |
| Primer: Fn-1 Reverse: GTCTACTCCACCGAACAACAA | This article | N/A |
| Primer: Tgfb-1 Forward: AGAGCCCTGGATACCAACTA | This article | N/A |
| Primer: Tgfb-1 Reverse: CAACCCAGGTCCTTCCTAAAG | This article | N/A |
| Primer: VEGFA Forward: AGGCTGCTGTAACGATGAAG | This article | N/A |
| Primer: VEGFA Reverse: TCTCCTATGTGCTGGCTTTG | This article | N/A |

**Continued**

| REAGENT or RESOURCE | SOURCE | IDENTIFIER |
|---|---|---|
| Primer: Lgals-3 Forward: ACACGAAGCAGGACAATAACT | This article | N/A |
| Primer: Lgals-3 Reverse: CAGCTTCAACCAGGACTTGTA | This article | N/A |
| Software and algorithms | | |
| ImageJ | NIH ImageJ software | ImageJ; RRID: SCR_003070 |
| GraphPad Prism 7 Software | GraphPad Software, | GraphPad, RRID: SCR_000306 |

## RESOURCE AVAILABILITY

### Lead contact

Further information and requests should be directed to and will be fulfilled by the lead contact: Jean X. Jiang (jiangj@uthscsa.edu)

### Materials availability

This study did not generate new animal models and reagents.

### Data and code availability

Not applicable.

## EXPERIMENTAL MODEL AND SUBJECT DETAILS

### dKO mice deficient of both Cx50 and AQP0

The breeding pairs of the Cx50 and AQP0 knockout mouse strain were generously provided by Dr. Thomas White at Stony Brook University and Dr. Alan Shiels at Washington University School of Medicine, respectively. The dKO mice deficient in both Cx50 and AQP0, Cx50 (-/-)/AQP0 (-/-) were generated by crossing C57BL/6 Cx50 (-/-) mice with C57BL/6 AQP0 (-/-) mice. Genotyping was performed by PCR technique using genomic DNA isolated from mouse tails and corresponding primers synthesized at the University of Texas Health Science center at San Antonio (UTHSCSA) Institutional DNA Core Facility. All mice were maintained in a pathogen-free environment at the AAALAC-accredited UTHSCSA animal facility following the NIH Guidelines for the Care and Use of Laboratory Animals. All animals were handled in accordance with the ARVO Statement for the Use of Animals in Ophthalmic and Vision Research and institutional protocols. The Institutional Animal Care and Use Committee (IACUC) approved the animal experimental protocols. The experiments were conducted blindly for WT and KO mouse models, and identity of the mice became available after completion of the data analysis.

## METHOD DETAILS

### Materials

Rat anti-mouse CD68 polyclonal antibody was obtained from BIO-RAD (Hercules, CA, USA). Monoclonal mouse anti-human smooth muscle actin antibody was obtained from Agilent (Santa Clara, CA, USA). Goat anti-connexin 46 polyclonal antibody was obtained from Santa Cruz (Dallas, TX, USA). Rabbit cleaved caspase-3 (Asp175) antibody was obtained from Fisher Scientific (Pittsburgh, PA, USA). Rabbit cleaved caspase-8 (NB100-56116) antibody, rabbit RIPK3/RIP3 (NBP1-77299) antibody, rabbit iNOS polyclonal (NB300605) antibody, and goat arginase 1 (NB10059740) antibody were obtained from Novus Biologicals (CO, USA). CSF-1 (mouse) recombinant protein (P4588) was obtained from Abnova (Taipei, Taiwan). Anti-mouse CSF1R (AFS98, BE0213) monoclonal antibody was obtained from Fisher Scientific (Pittsburgh, PA, USA). IHC adhesive glass slides (TOMO, Japan), High-Capacity RNA-to-cDNA Kit, and Maxima SYBR green/ROX qPCR master mix kit were obtained from Fisher Scientific. All other chemicals were obtained from either Sigma-Aldrich (St. Louis, MO, USA) or Fisher Scientific.

### Measurements of eye size and lens weight

Both male and female mice including WT and Cx50(-/-), AQP0(-/-), and dKO mice at various ages were euthanized in accordance with IACUC guidelines. Eyeballs were isolated and kept in 37°C prewarmed

phosphate-buffered saline (PBS) solution. Mouse lenses were carefully isolated from the posterior side. Images of pupil and lens were taken with both coronal and sagittal view using a standard dissection microscope. The diameters of pupils, eyeballs, and lenses at the equator were measured using NIH ImageJ software. The weight and diameter and of lenses of WT, Cx50 KO, AQP0 KO and dKO mice were determined at P 1, 7, 15, 30, 60, and 90 days. The ratio of lens weight to volume was calculated. P 1 day: WT, n=19; AQP0 KO, n=22; Cx50 KO, n=20; dKO, n=13. P 7 days: WT, n=17; AQP0 KO, n=19; Cx50 KO, n=16; dKO, n=14. P 15 days: WT, n=22; AQP0 KO, n=17; Cx50 KO, n=28; dKO, n=30. P 30 days: WT, n=14; AQP0 KO, n=16; Cx50 KO, n=14; dKO, n=20. P 60 days: WT, n=12; AQP0 KO, n=12; Cx50 KO, n=14; dKO, n=11. P 90 days: WT, n=19; AQP0 KO, n=18; Cx50 KO, n=13; dKO, n=20.

### Tissue paraffin sections and hematoxylin and eosin staining

A small hole (~ 1 mm diameter) behind the limbus was made in isolated eyeballs kept in PBS using a needle (BD Lo-Dose U-100 Insulin Syringes, Frankin Lake, USA). The whole eyeball was fixed in Fekete's acid-alcohol-formalin at room temperature for 24 h, dehydrated with ethanol and xylene, and embedded in paraffin. Sagittal sections (~ 3-μm thickness) were prepared. The tissue sections were mounted to adhesive glass slides, and stained with H&E. All of images were recorded by a Keyence BZ-X710 All-in-One fluorescence microscope with 20X and 60X objective lens.

### Frozen lens tissue sections and fluorescence microscopy

A small incision (~ 1 mm diameter) behind limbus was made in isolated eyeballs kept in PBS using a needle (BD Lo-Dose U-100 Insulin Syringes). The entire eyeball was fixed in 0.75% paraformaldehyde at room temperature for 24 h, washed with PBS 3 times (every time 30 min), immersed in 10%, and then, 20% sucrose solution for 1 h each, kept in 30% sucrose at 4°C overnight and then embedded in OCT compound (Sakura, Torrance, CA, USA). Sagittal sections (20 μm) stained with primary antibodies including anti-CD68 (1:500 dilution), anti-SMA (1:50 dilution), anti-Cx46 (1:200 dilution), anti-caspase-3 (1:50 dilution), anti-caspase-8 (1:100 dilution), anti-RIP3 (1:200 dilution), anti-iNOS (1:100 dilution), and anti-Arg1 (1:200 dilution) for 1 h at room temperature or 4°C overnight. Secondary antibodies were conjugated to Alexa Fluor 488 (1:400 dilution), Alexa Fluor 594 (1:400 dilution), or Alexa Fluor 647 (1:400 dilution) for 1 hr at room temperature, followed by 4′, 6-diamidino-2-phenylindole (DAPI) 0.2 μg/ml for 5 min at room temperature. Images were captured on the Keyence BZ-X710 All-in-One fluorescence microscopy.

### Immunohistochemistry staining

Paraffin sections were deparaffinized in xylene and alcohol and then incubated in citric acid antigen retrieval buffer (pH 6.0) for 2 h at 65°C. Samples were then incubated in 3% hydrogen peroxide solution for 20 min at room temperature to quench intrinsic peroxidase activity. To minimize nonspecific binding of antibodies, sections were incubated in Bloxall Blocking Solution (BA-2000; Vectastain ABC Kit, CA, USA) for 20 min and followed by staining with primary antibodies against α-SMA (1:100 dilution) for 30 min at room temperature and incubation with biotinylated secondary antibody and ABC Reagent for 30 min each at room temperature using the DAB peroxidase substrate kit (SK-4100; Vector Laboratories, CA, USA).

### Isolation of RNA from lens tissues and RT-qPCR

Real-time PCR was performed with total RNA isolated from the lens to detect messenger RNA expression of CD68, Arg-1, CSF-1, and Fn1. Lenses were isolated from the whole eyeball carefully in PBS. The lens samples were then pulverized using a frozen mortar and pestle in liquid nitrogen. Total RNA was extracted using TRI Reagent (Molecular Research Center, Cincinnati, OH, USA) as per the manufacturer's instructions. qPCR was performed using an ABI 7900 PCR device (Life Technologies, Carlsbad, CA, USA) and SYBR Green (Life Technologies) with a two-step protocol (94°C for 15 s and 64°C for 60 s). The ΔΔCT method was used for RT-qPCR data analysis. The primers of CD68 were as follows: sense, 5′-CCCACCTGTCTCTCT-CATTTC-3′ and antisense, 5′-GTATTCCACCGCCATGTAGT-3′. The primers of Arg-1 were as follows: sense, 5′-CAGAGGTCCAGAAGAATGGAAG-3′ and antisense, 5′-TCCACCCAAATGACACATAGG-3′. The primers of CSF-1 were as follows: sense, 5′-CAGGTGGAACTGCCAGTATAG-3′ and antisense, 5′-GAA-GATGGTAGGAGAGGGTAGT-3′. The primers of Fn-1 were as follows: sense, 5′-TCCTGTCTACCTCACA-GACTAC-3′ and antisense, 5′-GTCTACTCCACCGAACAACAA-3′. β-actin was used as a housekeeping gene control.

### Intravitreal injection

Injection into the vitreous cavity was performed using 33-gauge needles and micropipette on the right eye as described previously (Kubota et al., 2009; Gerhardt et al., 2003). Briefly, WT and dKO mice were anesthetized by intraperitoneal injection of xylazine (20 mg/kg) and ketamine (100 mg/kg) on P15. Levofloxacin was applied on the eye surface to prevent infection. Injection was performed under an ophthalmic operating microscope with micropipette at a point approximately 1 mm behind limbus. 0.1 mg/kg CSF-1, 25 mg/kg CSF-1 receptor antagonist (AFS98), or saline 0.5 μl was injected in vitreous cavity.

### Measure the number of macrophages and thickness of anterior capsule

Twenty continuous sagittal sections (~12-μm thickness) around central regions of whole eyeball were prepared, and three sections with the largest lens area were selected for immunofluorescence staining. After the staining, we captured the fluorescence images by Keyence BZ-X710 All-in-One fluorescence microscopy and analyzed the images in different areas including "tail-like" tissues, inside the lens and a sum of them as the total using counting number tools of NIH ImageJ software. The thickness of H&E-stained midsagittal paraffin lens sections of WT and dKO mice at P 15 and 60 days and 1 year was quantified. Nine locations along anterior capsule in each section were selected to obtain the mean value using measuring length tools of NIH ImageJ software.

## QUANTIFICATION AND STATISTICAL ANALYSIS

All data were analyzed with GraphPad Prism 7 Software (GraphPad Software, La Jolla, CA). ANOVA software followed by Tukey or Bonferroni was performed. The data were presented as the mean $\pm$ SEM of at least three measurements. Statistical significance was designated for analyses with $P < 0.05$. Asterisks in all figures indicate the degree of significant differences compared to controls, *, $P < 0.05$; **, $P < 0.01$; ***, $P < 0.001$; ****, $P < 0.0001$.